



## Nonclassical Nucleation in a Solid-Solid Transition of Confined Hard Spheres

Weikai Qi (齐维开),<sup>1,2</sup> Yi Peng (彭毅),<sup>3</sup> Yilong Han (韩一龙),<sup>3</sup> Richard K. Bowles,<sup>2</sup> and Marjolein Dijkstra<sup>1,\*</sup>

<sup>1</sup>*Soft Condensed Matter, Debye Institute for Nanomaterials Science, Department of Physics, Utrecht University, Princetonplein 5, 3584 CC Utrecht, The Netherlands*

<sup>2</sup>*Department of Chemistry, University of Saskatchewan, Saskatoon, Saskatchewan S7N 5C9, Canada*

<sup>3</sup>*Department of Physics, Hong Kong University of Science and Technology, Clear Water Bay, Hong Kong, China*

(Received 2 July 2015; published 29 October 2015)

A solid-solid phase transition of colloidal hard spheres confined between two planar hard walls is studied using a combination of molecular dynamics and Monte Carlo simulation. The transition from a solid consisting of five crystalline layers with square symmetry ( $5\Box$ ) to a solid consisting of four layers with triangular symmetry ( $4\Delta$ ) is shown to occur through a nonclassical nucleation mechanism that involves the initial formation of a precritical liquid cluster, within which the cluster of the stable  $4\Delta$  phase grows. Free-energy calculations show that the transition occurs in one step, crossing a single free-energy barrier, and that the critical nucleus consists of a small  $4\Delta$  solid cluster wetted by a metastable liquid. In addition, the liquid cluster and the solid cluster are shown to grow at the planar hard walls. We also find that the critical nucleus size increases with supersaturation, which is at odds with classical nucleation theory. The  $\Delta$ -solid-like cluster is shown to contain both face-centered-cubic and hexagonal-close-packed ordered particles.

DOI: 10.1103/PhysRevLett.115.185701

PACS numbers: 64.70.K-, 64.60.qe, 82.60.Nh

The kinetics of phase transitions plays an important role in condensed-matter physics and materials science. In order to gain a better fundamental understanding of how to control self-assembly processes in the fabrication of novel structures, many experimental and simulation studies have been devoted to colloidal systems. Experiments [1–4] and computer simulations [5–7] on bulk hard-sphere colloids suggested that the metastable fluid crystallizes and superheated crystals melt via a single-step nucleation process that is well described by classical nucleation theory (CNT) [8]. However, Ostwald’s step rule suggests that the kinetic pathway to the most stable state can initially proceed through the nucleation of intermediate, metastable phases [9]. The effect of a nearby metastable state on nucleation and the occurrence of multistep nucleation processes have been studied in the crystallization of a range of systems including colloids [10,11], proteins [12], and patchy particles [13], and in the crystallization of molecular solids from solution [14].

In contrast, the kinetic processes of solid-solid phase transitions, which involve complex structural rearrangements [15], have received considerably less attention [16]. Solid-solid transitions usually occur in a martensitic fashion [17,18] involving the concerted, diffusionless motion of the atoms in the unit cell. Anisotropic stress, rapid quenching, and a small system size have been found to promote martensitic transformations [19]. In colloids, martensitic transitions have been observed in small crystalline clusters [20–22] or lattices stretched by external fields [18,23–25]. A solid-solid transition involving an activated nucleation process has recently been experimentally observed at the single-particle level for the first time in colloidal thin-film

crystals confined between two glass plates [26]. The equilibrium phase diagram of hard spheres confined between two planar hard walls shows an alternating sequence of solid-solid transitions,  $\dots n\Delta \rightarrow (n+1)\Box \rightarrow (n+1)\Delta \dots$ , as the plate separation increases [27–30], where  $n$  is the number of crystalline layers. Peng *et al.* [26] found that the transition from the  $(n+1)\Box$  crystal to the  $(n)\Delta$  crystal followed Ostwald’s step rule and occurred via a two-step nucleation process involving an intermediate liquid phase.

We study the nucleation mechanism of the  $5\Box \rightarrow 4\Delta$  solid-solid transition in a system of hard spheres of diameter  $\sigma$  confined between two parallel hard plates separated by a distance  $H/\sigma = 4$ , using computer simulations. Our simulations are carried out in the packing fraction range  $0.479 < \eta < 0.500$  (i.e., the 2D reduced lateral pressure range  $35.8 < P^* = \beta P \sigma^2 < 40$ ), where the  $5\Box$  crystal and the liquid phase are metastable with respect to the  $4\Delta$  crystal (see the Supplemental Material [31] for details). The free energy of the liquid phase lies between the free energies of the two solid phases.  $\beta = 1/(k_B T)$  denotes the inverse temperature, with  $T$  being the temperature and  $k_B$  being the Boltzmann constant. In order to explore the role a metastable liquid phase might play in this solid-solid transition, we calculate the free energy of formation for a cluster containing  $N_L$  liquidlike particles and  $N_\Delta$  solidlike particles with triangular symmetry. The resulting free-energy surface shows that the optimal kinetic pathway for the transition entails the initial growth of a liquid cluster, within which the  $\Delta$ -solid cluster forms, but there is only one nucleation barrier involving a critical cluster consisting of liquid- and solidlike particles in our parameter regime.

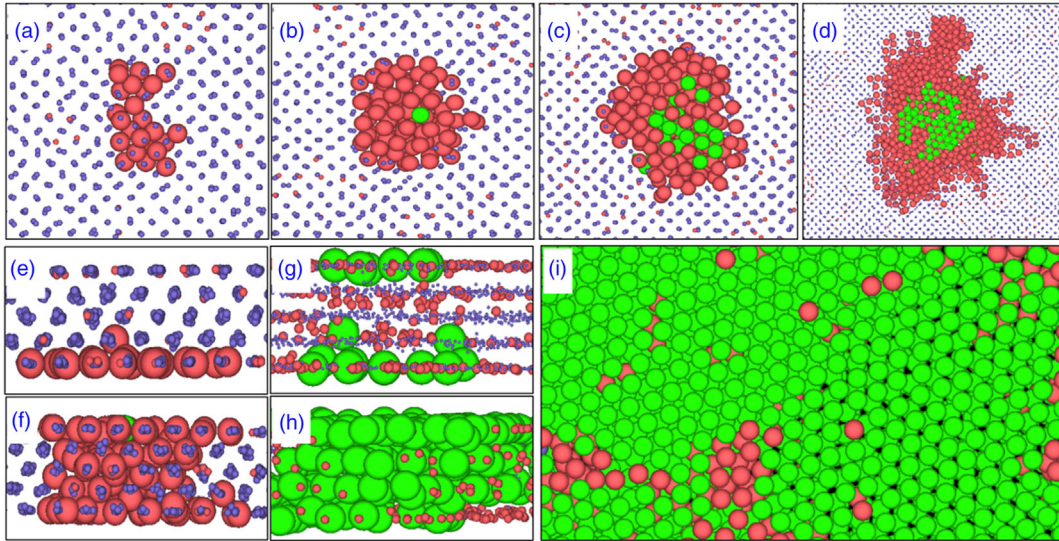


FIG. 1 (color online). Typical configurations of the solid-solid transition. Configurations obtained by umbrella sampling in MC simulations with a bias towards cluster sizes of (a)  $N_{\text{cl}} = 60$ , (b)  $N_{\text{cl}} = 120$ , and (c)  $N_{\text{cl}} = 180$  particles. (d) A configuration obtained by EDMD simulation at  $t = 518\tau$  for  $\eta = 0.490$ . Side (e) and top (f) views of a liquid nucleus in an EDMD simulation. Side (g) and top (h) views of a  $\Delta$ -solid nucleus in an EDMD simulation. (i) A solid consisting of four  $\Delta$  layers arranged in both fcc and hcp structures from EDMD simulations. In (a)–(d), multilayer particles are projected onto the  $xy$  plane.  $\square$ -solid,  $\Delta$ -solid and liquidlike particles are colored in blue, green, and red, respectively. Particles not belonging to the largest cluster are drawn small.

To distinguish between fluidlike and solidlike particles with square ( $\square$ ) and triangular ( $\Delta$ ) symmetries, we calculate the bond orientational order  $\psi_{mj} = \sum_{k=1}^{N_b(j)} \exp(im\theta_k) / N_b(j)$  of each particle  $j$  with  $m = 4, 6$  for solidlike particles with four- and sixfold symmetries, where  $\theta_j$  is the angle between the bond of particles  $i$  and  $j$  with an arbitrary reference axis, and  $N_b(j)$  denotes the number of nearest neighbors of particle  $j$  [34]. We divide the system into five and four layers for the calculation of  $\psi_4$  and  $\psi_6$ , respectively. In addition, a crystalline bond with  $m$ -fold symmetry is defined if  $|\psi_{mi}^* \cdot \psi_{mj}| > 0.5$  [26]. We define particles as  $\Delta$ -solid-like if the number of crystalline bonds with triangular symmetry  $\xi_{\Delta} \geq 3$ , and as  $\square$ -solid-like if the number of crystalline bonds with square symmetry  $\xi_{\square} \geq 2$ . All other particles are defined as liquidlike. The criteria guarantee that no particle is both  $\square$ -solid-like and  $\Delta$ -solid-like. Liquid- and  $\Delta$ -solid-like particles are considered to belong to the same cluster if the distance between any two particles is less than  $1.5\sigma$ .

We perform Monte Carlo (MC) simulations using the umbrella sampling technique in the isothermal-isobaric ( $NPT$ ) ensemble, with the number of particles  $N = 2000$ , the reduced 2D lateral pressure  $P^* = 40$ , and the temperature  $T$  fixed. Figure 1(a)–1(c) show typical configurations along the nucleation pathway in MC simulations. Nucleation studies usually focus on a one-dimensional free-energy barrier using the total cluster size,  $N_{\text{cl}}$ , as the reaction coordinate. Hence, we calculate the free energy,  $\beta\Delta G(N_{\text{cl}}) = -\log \mathcal{P}(N_{\text{cl}})$ , where  $\mathcal{P}(N_{\text{cl}})$  is the probability of observing a cluster of size  $N_{\text{cl}} = N_L + N_{\Delta}$ .

We use two different biasing potentials:  $W(N_{\text{cl}}) = \frac{1}{2}k(N_{\text{cl}} - N_{\text{cl}0})^2$  and  $W(N_L) = \frac{1}{2}k(N_L - N_{L0})^2$ . The first biasing potential is designed to follow the growth of a binary cluster and the second the possible nucleation of a liquid cluster, but we stress that the potential does not prevent the growth of  $\Delta$ -solid-like particles.  $N_{\text{cl}0}$  and  $N_{L0}$  are the umbrella window centers for the total cluster size and the number of liquid particles in the cluster, respectively. The sampling is performed using 60 umbrella centers, equally spaced in the region  $N_{\text{cl}}, N_L \in [0, 300]$ . For each umbrella window, the data are harvested from 10000 equilibrium configurations and averaged over ten independent runs. The free energies from each umbrella window are combined into a single curve using the multistage Bennet acceptance ratio method [35].

Figure 2 shows that the two biasing schemes give similar free energies for cluster sizes up to  $\sim 100$ , where the cluster consists solely of liquidlike particles [Figs. 1(a) and 1(b)]. At larger cluster sizes, the two free-energy curves begin to diverge with the emergence of  $\Delta$ -solid-like particles in the  $N_{\text{cl}}$  biasing scheme but not in the  $N_L$  biasing scheme, which suggests a degree of hysteresis. If both schemes were fully equilibrated, we would expect them to yield similar free energies, but the newly emerged  $\Delta$ -solid particles are not easily sampled when the  $N_L$  biasing potential is employed.  $N_{\Delta}$  increases rapidly for both biasing schemes at the free-energy maximum, where  $N_{\text{cl}}^* \sim 175$ , but Fig. 2(b) also shows that  $N_{\Delta}$  is already increasing, even before the maximum under  $N_{\text{cl}}$  biasing.

More insight into the nucleation mechanism can be obtained by calculating the two-dimensional free-energy

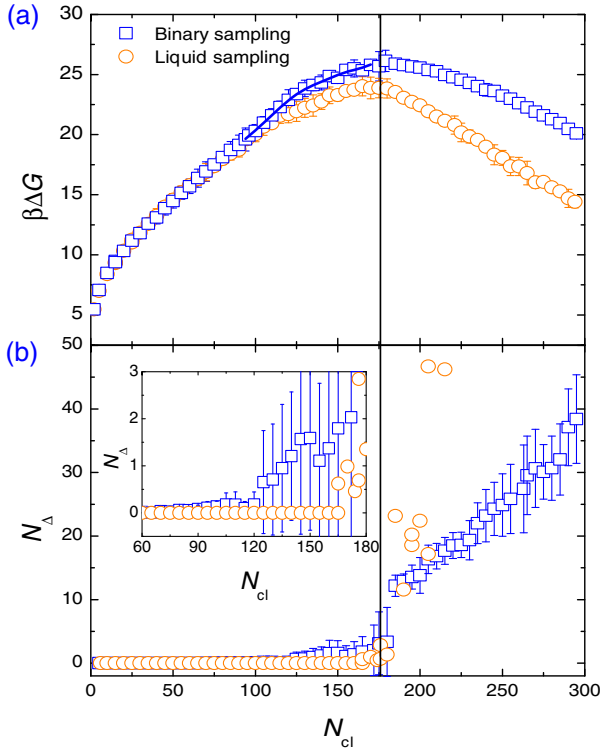


FIG. 2 (color online). (a) The Gibbs free energy  $\Delta G(N_{cl})/(k_B T)$  as a function of the total number of particles  $N_{cl}$  using the  $W(N_{cl})$  biasing potential (the squares) and the  $W(N_L)$  biasing potential (the circles). (b) Number of  $\Delta$ -like particles  $N_{\Delta}$  averaged over 10000 nuclei as a function of cluster size  $N_{cl}$  as obtained from the two biasing methods. (Inset) The same plot as (b) but with the region  $60 < N_{cl} < 180$  enlarged for clarity. The vertical line marks the critical nucleus size.

surface of forming a cluster containing  $N_L$  and  $N_{\Delta}$  particles,  $\beta\Delta G(N_L, N_{\Delta}) = -\log P(N_L, N_{\Delta})$ , where  $P(N_L, N_{\Delta})$  denotes the probability of observing the largest cluster in the system with  $(N_L, N_{\Delta})$ . We perform MC simulations using umbrella sampling in the  $NPT$  ensemble, at the same thermodynamic conditions, and use a quadratic biasing potential,  $W(N_L, N_{\Delta}) = \frac{1}{2}[k_L(N_L - N_{L0})^2 + k_{\Delta}(N_{\Delta} - N_{\Delta0})^2]$  [36], where  $\beta k_L = 0.15$  and  $\beta k_{\Delta} = 0.3$ . A total of 300 umbrella windows are used, with adjacent umbrella window centers separated by five particles, covering the ranges  $N_{L0} \in [0, 250]$  and  $N_{\Delta0} \in [0, 30]$ . For each umbrella window, the system is equilibrated for  $10^7$  MC steps before data are collected over the next  $2 \times 10^6$  MC steps, harvesting configurations every 200 MC steps. We present the contour plot of the free-energy surface in the  $N_L - N_{\Delta}$  plane in Fig. 3. We see a significant increase in the free energy of growing pure liquidlike clusters beyond  $N_L \approx 170$ , and we do not find a saddle point leading to the nucleation of the pure liquid phase. Instead, the lowest free-energy path on the surface shows that a  $\Delta$ -solid-like cluster starts growing inside the pre-critical liquid cluster and that the critical embryo contains

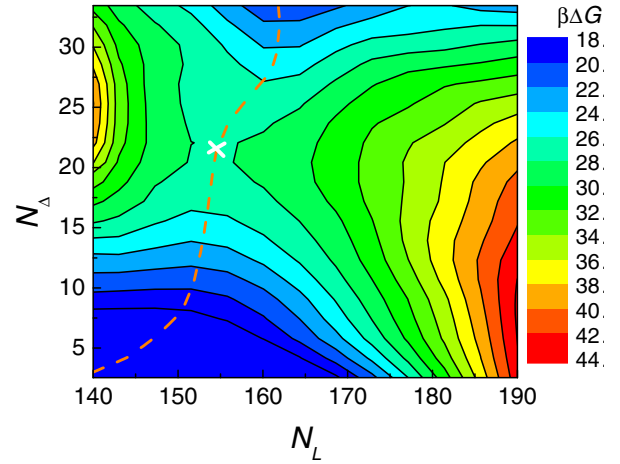


FIG. 3 (color online). Contour plot of  $\beta\Delta G(N_L, N_{\Delta})$  in the saddle point region. The nucleation barrier height  $\beta\Delta G^* \approx 26$  and the critical cluster (the white cross) contains  $N_L = 155$  liquidlike particles and  $N_{\Delta} = 22$   $\Delta$ -solid-like particles. The lowest free-energy path through the saddle point region is indicated by the dashed orange curve.

$N_{\Delta} \approx 25$  solidlike particles surrounded by  $N_L \sim 155$  liquidlike particles [Fig. 1(c)]. Beyond the nucleation saddle point, the new phase continues to grow as  $N_{\Delta}$  and  $N_L$  both increase [Fig. 1(d)]. A key feature of our free-energy surface is the presence of a single free-energy barrier leading to the  $\Delta$  crystal, which suggests that the transition occurs in a single step, even though a liquid cluster is developed in the initial stages of the nucleation process. The free-energy surface has a similar form to that obtained by ten Wolde and Frenkel [12] in their study of protein crystallization. They showed that the lowest free-energy path proceeds via the formation of a liquidlike droplet, within which a crystallite starts to form.

A simple CNT for our system, where the nucleus has a cylindrical core of  $\Delta$ -solid particles surrounded by a layer of liquid particles, exhibits a two-step mechanism (see Fig. S6). A saddle point associated with a pure liquid critical cluster leads to the liquid free-energy basin, which is then separated from the  $\Delta$ -crystal basin by a ridge on the free-energy surface, so nucleation requires the crossing of two barriers. Accounting for the disjoining pressure [37,38] associated with the thin wetting layer and the strain energy of the lattice [15], the CNT introduces a saddle point on the free-energy surface with a liquid- $\Delta$ -solid critical cluster leading directly to the crystal phase, as observed in our simulations, but the valley floor approaching this saddle point, and hence the precritical fluctuations, grows along the  $\Delta$ -solid axis. In our simulation results, the early stages of nucleation are characterized by the formation of pure liquidlike clusters, which is at odds with CNT.

Finally, we use event-driven molecular dynamics (EDMD) simulations in the canonical ( $NVT$ ) ensemble to obtain the dynamics of the nucleation process, starting

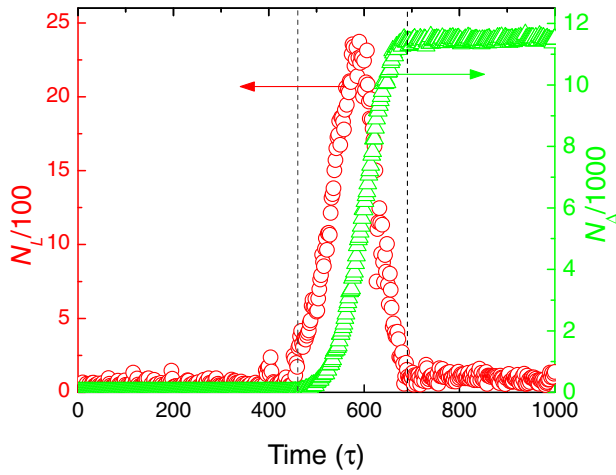


FIG. 4 (color online). The number of liquidlike particles (left),  $N_L$ , and  $4\Delta$  like particles (right),  $N_\Delta$ , in the largest cluster as a function of time  $t$  in MD time units.

from a metastable defect-free  $5\Box$  phase. At  $\eta \geq 0.5$  (i.e.,  $P^* \geq 40$  in the  $5\Box$  phase), the EDMD runs never nucleate on the time scale of our simulations. Nucleation events begin when  $\eta$  is reduced to 0.49. A long induction period is observed during which the liquid cluster size fluctuates and the number of  $N_\Delta$  remains near zero (Fig. 4). The initial liquid cluster appears to form at the hard-wall interface in a heterogeneous fashion [Fig. 1(e)]. It then grows into a cylindrical nucleus spanning the two walls [Fig. 1(f)]. The  $\Delta$ -solid cluster forms within the fluctuating liquid also at the liquid-wall interface [Fig. 1(g)], which is consistent with studies of the prefreezing and crystallization of the bulk hard-sphere fluid at a hard-wall interface [39]. In our EDMD simulations, the number of liquid particles  $N_L$  surges to a maximum before decreasing as the liquid is consumed in the growth of the  $\Delta$ -nucleus [Figs. 1(h) and 4], which contains either face-centered-cubic (fcc) or hexagonal-close-packed (hcp) layering [Fig. 1(i)].

To further examine the possibility that the liquid and the  $\Delta$  crystal nucleate independently of each other, we estimate the nucleation rate by measuring the mean first passage time,  $\tau(N)$ , during the appearance of a cluster containing  $N = N_L$  or  $N = N_\Delta$  particles [40,41] (see the Supplemental Material [31] for more details). Figures 5(a) and 5(b) show that the mean first passage times for the liquid and the  $\Delta$  solid reach their plateaus at similar times, yielding a nucleation rate  $J = C_1/(2V) = 1.43 \times 10^{-7} \tau/\sigma^3$ , where  $V$  is the sample volume. At a lower  $\eta$ , the liquid nucleates slightly slower than the solid (see Table II in the Supplemental Material [31]), which indicates that the  $\Delta$  solid nucleates within a precritical liquid nucleus. Furthermore, the critical nucleus size is determined from the EDMD simulations as a function of  $\eta$ . According to CNT, the critical size of the liquid nucleus should decrease as  $\eta$  decreases (i.e., as the chemical potential difference between the liquid and the  $5\Box$  crystal

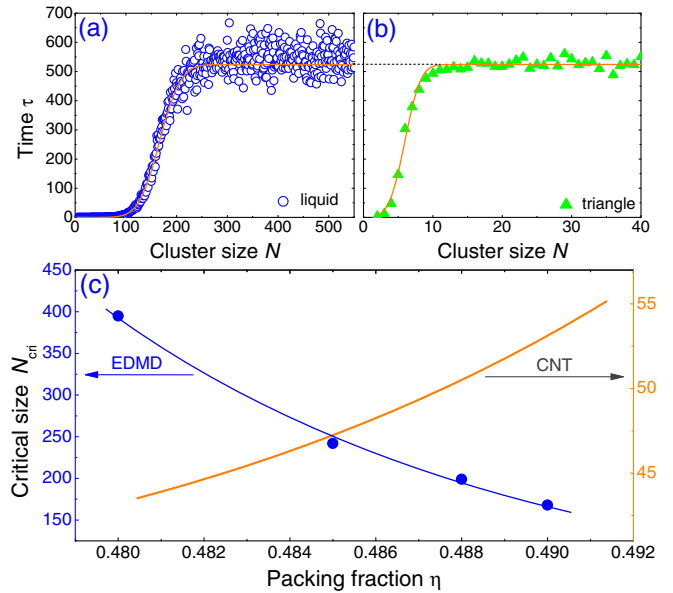


FIG. 5 (color online). The mean first passage time  $\tau(N)$  for (a) liquid and (b)  $4\Delta$  clusters in EDMD simulations at  $\eta = 0.490$ . Lines are fits of the mean first passage time using  $1/C_1\{1 + \text{erf}[C_2(N - N_{\text{cri}})]\}$  where  $\text{erf}$  is the error function [40,41]. For liquid clusters,  $C_1 = 0.00382$ ,  $C_2 = 0.02161$ , and  $N_{\text{cri}} = 167$ . For  $4\Delta$  clusters,  $C_1 = 0.00382$ ,  $C_2 = 0.39442$ , and  $N_{\text{cri}} = 6$ . (c) The critical size of the liquid nucleus as a function of the packing fraction calculated from the fitting of the mean first passage time in EDMD simulations (the blue dots) and classical nucleation theory (the orange line) (see the Supplemental Material [31], Sec. III).

increases). However, Fig. 5(c) shows the opposite trend: the number of liquid particles in the critical cluster actually increases. A possible explanation for this unconventional finding might be that the liquid clusters correspond to precritical fluctuations with a correlation length that increases as the limit of stability of the  $5\Box$  crystal is approached with respect to the liquid [12,42] (i.e., upon lowering the packing fraction  $\eta$ ).

Solid-solid transitions usually occur through a martensitic process when the driving force for nucleation is small and the barrier is high because it avoids the need to develop a solid-solid interface, which has a high free-energy cost. However, our simulations show that the  $5\Box \rightarrow 4\Delta$  solid-solid transition occurs via a nonclassical nucleation mechanism involving an intermediate liquid stage. This provides an alternative mechanism that also obviates the need to form a solid-solid interface. Furthermore, the initial nuclei should always be liquid if the  $\Delta - \Box$  interfacial free energy is higher than the sum of the  $\Delta$ -liquid and liquid- $\Box$  interfacial free energies since the interfacial free energy dominates over the bulk chemical potential difference when the nucleus is small enough. Since the mechanism is general, intermediate liquids could exist widely in other systems. For example, the interfacial energy in metals and alloys ranges from 500 to 1000  $\sim \text{mJ/m}^2$  for the incoherent

interfaces between two crystalline phases and from 30 to  $250 \sim \text{mJ}/\text{m}^2$  for solid-liquid interfaces [15]. Hence, an intermediate liquid stage could similarly exist in the solid-solid transformation of metals.

W. Q. and M. D. acknowledge financial support from a Nederlandse Organisatie voor Wetenschappelijk Onderzoek (NWO) VICI grant. W. Q. and R. K. B. thank NSERC and the Sylvia Fedoruk Canadian Centre for Nuclear Innovation for support and WestGrid for the computational resources. Y. H. acknowledges financial support from NSFC Grant No. 11374248.

\*M.Dijkstra1@uu.nl

- [1] K. Schätzel and B. J. Ackerson, *Phys. Rev. Lett.* **68**, 337 (1992).
- [2] B. J. Ackerson and K. Schätzel, *Phys. Rev. E* **52**, 6448 (1995).
- [3] U. Gasser, E. R. Weeks, A. Schofield, P. N. Pusey, and D. A. Weitz, *Science* **292**, 258 (2001).
- [4] Z. Wang, F. Wang, Y. Peng, Z. Zheng, and Y. Han, *Science* **338**, 87 (2012).
- [5] S. Auer and D. Frenkel, *Nature (London)* **409**, 1020 (2001).
- [6] L. Fillion, M. Hermes, R. Ni, and M. Dijkstra, *J. Chem. Phys.* **133**, 244115 (2010).
- [7] T. Kawasaki and H. Tanaka, *Proc. Natl. Acad. Sci. U.S.A.* **107**, 14036 (2010).
- [8] D. Turnbull and J. C. Fisher, *J. Chem. Phys.* **17**, 71 (1949).
- [9] W. Ostwald, *Z. Phys. Chem. (Leipzig)* **22**, 289 (1897).
- [10] H. J. Schöpe, G. Bryant, and W. van Meegen, *Phys. Rev. Lett.* **96**, 175701 (2006).
- [11] P. Tan, N. Xu, and L. Xu, *Nat. Phys.* **10**, 73 (2014).
- [12] P. R. ten Wolde and D. Frenkel, *Science* **277**, 1975 (1997).
- [13] L. O. Hedges and S. Whitelam, *J. Chem. Phys.* **135**, 164902 (2011).
- [14] D. Erdemir, A. Y. Lee, and A. S. Myerson, *Acc. Chem. Res.* **42**, 621 (2009).
- [15] D. A. Porter, K. E. Easterling, and M. Y. Sherif, *Phase Transformations in Metals and Alloys* (CRC Press, Boca Raton, FL, 2002).
- [16] U. Gasser, *J. Phys. Condens. Matter* **21**, 203101 (2009).
- [17] A. G. Khachaturyan, *Theory of Structural Transformation in Solids* (John Wiley & Sons, New York, 1983).
- [18] A. Yethiraj, A. Wouterse, B. Groh, and A. van Blaaderen, *Phys. Rev. Lett.* **92**, 058301 (2004).
- [19] R. Z. Khaliullin, H. Eshet, T. D. Kühne, J. Behler, and M. Parrinello, *Nat. Mater.* **10**, 693 (2011).
- [20] M. T. Casey, R. T. Scarlett, W. B. Rogers, I. Jenkins, T. Sinno, and J. C. Crocker, *Nat. Commun.* **3**, 1209 (2012).
- [21] I. C. Jenkins, M. T. Casey, J. T. McGinley, J. C. Crocker, and T. Sinno, *Proc. Natl. Acad. Sci. U.S.A.* **111**, 4803 (2014).
- [22] J. A. Weiss, D. W. Oxtoby, D. G. Grier, and C. A. Murray, *J. Chem. Phys.* **103**, 1180 (1995).
- [23] S. Nojd, P. S. Mohanty, P. Bagheri, A. Yethiraj, and P. Schurtenberger, *Soft Matter* **9**, 9199 (2013).
- [24] Y. Yang, L. Fu, C. Marcoux, J. E. S. Socolar, P. Charbonneau, and B. B. Yellen, *Soft Matter* **11**, 2404 (2015).
- [25] P. S. Mohanty, P. Bagheri, S. Nöjd, A. Yethiraj, and P. Schurtenberger, *Phys. Rev. X* **5**, 011030 (2015).
- [26] Y. Peng, F. Wang, Z. Wang, A. M. Alsayed, Z. Zhang, A. G. Yodh, and Y. Han, *Nat. Mater.* **14**, 101 (2015).
- [27] P. Pieranski, L. Strzelecki, and B. Pansu, *Phys. Rev. Lett.* **50**, 900 (1983).
- [28] M. Schmidt and H. Löwen, *Phys. Rev. Lett.* **76**, 4552 (1996).
- [29] S. Nesper, C. Bechinger, P. Leiderer, and T. Palberg, *Phys. Rev. Lett.* **79**, 2348 (1997).
- [30] A. Fortini and M. Dijkstra, *J. Phys. Condens. Matter* **18**, L371 (2006).
- [31] See Supplemental Material at <http://link.aps.org/supplemental/10.1103/PhysRevLett.115.185701>, which includes Refs. [32,33], for phase behavior, CNT model and nucleation rate calculations.
- [32] K. Zahn and G. Maret, *Phys. Rev. Lett.* **85**, 3656 (2000).
- [33] A. Härtel, M. Oettel, R. E. Rozas, S. U. Egelhaaf, J. Horbach, and H. Löwen, *Phys. Rev. Lett.* **108**, 226101 (2012).
- [34] D. R. Nelson, *Defects and Geometry in Condensed Matter Physics* (Cambridge University Press, Cambridge, England, 2009).
- [35] M. R. Shirts and J. D. Chodera, *J. Chem. Phys.* **129**, 124105 (2008).
- [36] S. Auer and D. Frenkel, *J. Chem. Phys.* **120**, 3015 (2004).
- [37] Y. S. Djikaev, R. Bowles, H. Reiss, K. Hämeri, A. Laaksonen, and M. Väkevä, *J. Phys. Chem. B* **105**, 7708 (2001).
- [38] M. Iwamatsu, *J. Chem. Phys.* **134**, 164508 (2011).
- [39] M. Dijkstra, *Phys. Rev. Lett.* **93**, 108303 (2004).
- [40] J. Wedekind, R. Strey, and D. Reguera, *J. Chem. Phys.* **126**, 134103 (2007).
- [41] S. E. M. Lundrigan and I. Saika-Voivod, *J. Chem. Phys.* **131**, 104503 (2009).
- [42] R. Ni, S. Belli, R. van Roij, and M. Dijkstra, *Phys. Rev. Lett.* **105**, 088302 (2010).

# Supplemental Materials for Nonclassical Nucleation in a Solid-Solid Transition of Confined Hard Spheres\*

Weikai Qi,<sup>1,2</sup> Yi Peng,<sup>3</sup> Yilong Han,<sup>3</sup> Richard K. Bowles,<sup>2</sup> and Marjolein Dijkstra<sup>1,\*</sup>

<sup>1</sup>*Soft Condensed Matter, Debye Institute for Nanomaterials Science, Utrecht University, Princetonplein 5, 3584 CC Utrecht, The Netherlands*

<sup>2</sup>*Department of Chemistry, University of Saskatchewan, Saskatoon, Saskatchewan S7N 5C9, Canada*

<sup>3</sup>*Department of Physics, Hong Kong University of Science and Technology, Clear Water Bay, Hong Kong, China*

(Dated: September 23, 2015)

## I. PHASE BEHAVIOR OF CONFINED HARD SPHERES: THE $5\Box \rightarrow 4\Delta$ TRANSITION

We consider a system consisting of  $N$  hard spheres of diameter  $\sigma$  confined between two parallel hard walls with a surface area  $A$  and separated by a distance  $H/\sigma = 4$ . The packing fraction for the system is defined as  $\eta = \pi N\sigma^3/(6AH)$ . According to free-energy calculations [1], the system exhibits a first-order phase transition from a liquid to a crystal phase consisting of four triangular layers ( $4\Delta$ ), and a first-order phase transition from the  $4\Delta$  crystal phase to a crystal phase consisting of five square layers ( $5\Box$ ) with a  $5\Box - 4\Delta$  phase coexisting regime  $0.537 < \eta < 0.571$ .

To obtain the chemical potential differences between the phases in the metastable regions of the phase diagram, we use event-driven molecular dynamics (EDMD) simulations to calculate the equation of state. In an EDMD simulation, the system evolves via a time-ordered sequence of elastic collision events, which are described by Newton's equations of motion. The spheres move at constant velocity between collisions, and their velocities are updated when a collision occurs. We compute the reduced 2D lateral pressure  $P^* = \beta P\sigma^2$  via the virial theorem,

$$P^* = \beta P\sigma^2 = \frac{N\sigma^2}{A} \left[ 1 - \frac{\beta m}{2t} \frac{1}{N} \sum_{i<j} \mathbf{r}_{ij} \cdot \mathbf{v}_{ij} \right], \quad (1)$$

where  $m = 1$  is the mass of the particles,  $N = 12500$  is the number of particles,  $\beta = 1/k_B T$ ,  $k_B$  is the Boltzmann constant,  $T$  is the temperature,  $\mathbf{r}_{ij}$  and  $\mathbf{v}_{ij}$  are respectively the displacement and velocity of particle  $i$  relative to those of particle  $j$ , and  $t$  is the time interval. Time is measured in MD units  $\tau = \sqrt{\frac{m\sigma^2}{k_B T}}$ . The system is equilibrated for  $800\tau$ , and the pressure is measured for an additional  $200\tau$ . Figure S1 shows the equations of states obtained from the simulation.

In this work, we study the kinetics of the phase transition from a metastable  $5\Box$ -crystal to a stable  $4\Delta$ -crystal phase. A phase diagram in the literature shows that for  $\eta < 0.571$ , the  $4\Delta$ -crystal phase is thermodynamically

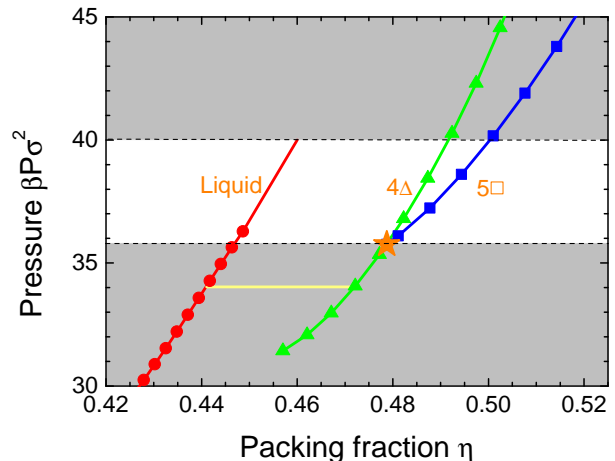


FIG. S1. Equations of states (i.e. the reduced 2D lateral pressure  $P^* = \beta P\sigma^2$  as a function of packing fraction  $\eta$ ) of the liquid (dots),  $4\Delta$  crystal (triangles) and  $5\Box$  crystal (squares) phases in a system of hard spheres confined between two planar hard walls separated by a distance  $H/\sigma = 4$ . Curves are the fifth degree polynomial fittings of equations of states of the liquid (red),  $4\Delta$  crystal (green) and  $5\Box$  crystal (blue) phases. The yellow line indicates the region where the liquid and  $4\Delta$  crystal phases coexist and the star indicates the point where the pressure is the same for both the  $4\Delta$  and  $5\Box$  crystal phases. Our nucleation study is carried out in the region  $35.8 \leq P^* \leq 40$  (white area between the dotted lines).

stable as its free energy is lower than that of the  $5\Box$  phase [1]. Using the  $5\Box$ -crystal phase as the initial configuration in our simulations, we find that this phase remains metastable down to a pressure  $P^* = 35.8$ , which corresponds to a packing fraction  $\eta = 0.479$ . We also note that at  $\eta = 0.479$ , both the  $4\Delta$  and  $5\Box$  crystals have the same pressure  $P^* = 35.8$ . The  $5\Box$ -crystal phase is thus metastable in the region  $0.479 < \eta < 0.571$ . Due to the limited simulation time, a critical nucleus cannot form in the  $5\Box \rightarrow 4\Delta$  transition at  $\eta > 0.500$ . We calculate the chemical potentials of each phase using thermodynamic integration along the equation of state. For  $\eta \leq 0.500$ , the chemical potential difference between the  $5\Box$ -solid and liquid phases,  $\mu_{\Box-L}$ , decreases with increasing packing fraction  $\eta$  (see Table 1 or Fig. S2). This reduces the thermodynamic driving force for nucleation and lowers the probability of observing liquid droplets through density fluctuations in our simulations. As a result, we

\* M.Dijkstra1@uu.nl

$P^*$	$\eta_L$	$\eta_\Delta$	$\eta_\square$	$\beta\mu_L$	$\beta\mu_\Delta$	$\beta\mu_\square$	$\beta\mu_{\square-L}$	$\beta\mu_{L-\Delta}$
40	0.460	0.492	0.500	15.14	15.02	15.34	0.20	0.12
39	0.457	0.489	0.496	14.85	14.75	15.08	0.23	0.10
38	0.454	0.486	0.491	14.56	14.48	14.81	0.25	0.08
37	0.451	0.483	0.487	14.27	14.21	14.54	0.27	0.06

TABLE I. Pressure  $P^* = \beta P \sigma^2$ , packing fraction  $\eta$  and chemical potentials  $\beta\mu$  for the liquid,  $4\Delta$ -solid and  $5\square$ -solid phases.  $\beta\mu_{\square-L}$  is the chemical potential difference between  $5\square$  and the liquid, and  $\beta\mu_{L-\Delta}$  is the chemical potential difference between the liquid and the  $4\Delta$ -solid phase.

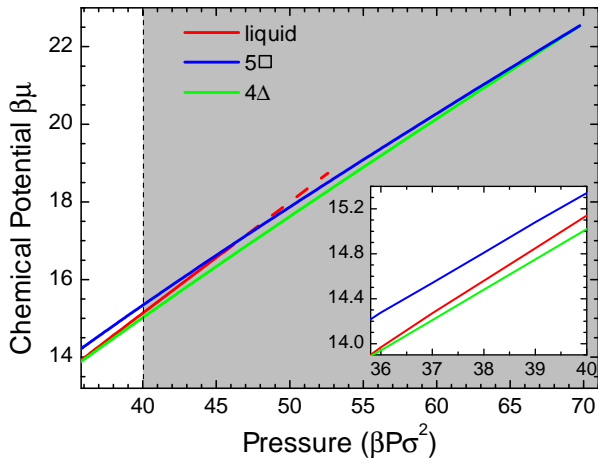


FIG. S2. Chemical potentials  $\beta\mu$  for the liquid,  $4\Delta$  and  $5\square$  phases in the region  $35.8 < P^* < 70$  where the liquid and  $5\square$  are metastable. Inset shows chemical potentials in the region  $35.8 \leq P^* \leq 40$ .

focus on nucleation in the region  $0.479 \leq \eta \leq 0.500$  or  $35.8 \leq P^* \leq 40$ .

## II. FORMATION OF A LIQUID DROPLET IN THE SOLID-SOLID TRANSITION

In the EDMD simulations, the defect-free  $5\square$ -solid phase at packing fraction  $\eta = 0.490$  developed small liquid-like clusters which fluctuated in size. After a long induction time, a critical liquid nucleus appeared embedding a  $4\Delta$ -nucleus. The bond orientational order parameter  $\Psi_6$  has been used to distinguish among the fluid-,  $4\Delta$ -, and  $5\square$ -like particles in the main text. However, as the liquid-like particles move much faster than the crystalline particles, one can also employ a dynamic criterion. To this end, we measure the self-part of the Van Hove correlation function as defined by [2]

$$G_s(R, t) = \frac{1}{N} \left\langle \sum_i^N \delta(R - |\mathbf{R}_i(t + t_w) - \mathbf{R}_i(t_w)|) \right\rangle, \quad (2)$$

where  $\mathbf{R}_i(t)$  is the position of particle  $i$  at time  $t$ , and  $R$  the diffusion distance of the particles during time interval  $t$ . At short waiting times, the Van Hove correlation function is Gaussian. As soon as a liquid nucleus starts to

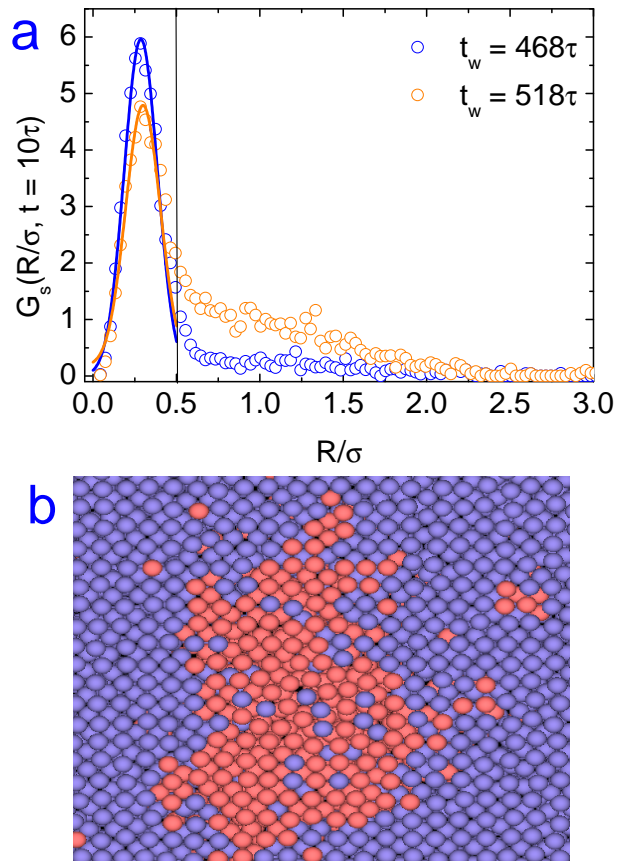


FIG. S3. (a) Self-part of the Van Hove correlation function  $G(R, t = 10\tau)$  at waiting times  $t_w = 468\tau$  and  $t_w = 518\tau$ . The vertical line marks the non-Gaussian long tails corresponding to the fast-moving particles. Solid curves are the Gaussian fits. (b) A typical configuration at waiting time  $t_w = 518\tau$  of the EDMD simulation at packing fraction  $\eta = 0.490$ . The red and blue particles denote the fast-moving and slow-moving particles, respectively.

grow at waiting times  $t_w = 468\tau$  and  $518\tau$ , the Van Hove correlation function becomes non-Gaussian as shown in Fig. S3a. The long tail of the self-part of the Van Hove correlation function indicates the presence of liquid-like particles with higher mobilities than the solid-like particles. In Fig. S3b, the fast-moving particles, i.e. those with displacement  $> 0.5\sigma$  in a time interval  $t = 10\tau$ , correspond to disordered fluid-like particles, which confirms

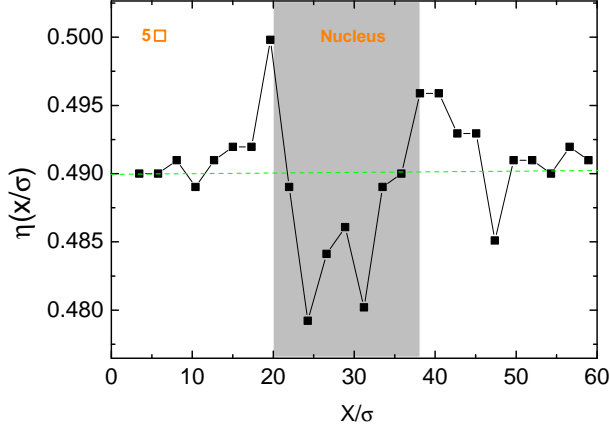


FIG. S4. The density profile across the diameter of the cluster at waiting time  $t_w = 518\tau$  in MD time units and at a packing fraction  $\eta = 0.490$ . The green dashed line denotes the packing fraction of the metastable  $5\square$  phase. The location of the liquid- $4\Delta$  nucleus is denoted by the shaded region.

the formation of a liquid-like droplet in the nucleation process. In addition, the density profile of the cluster in Fig. S4 confirms the formation of a liquid-like droplet. The packing fraction a long way from the nucleus approaches that of the metastable  $5\square$  phase.

### III. CLASSICAL NUCLEATION THEORY FOR THE $5\square \rightarrow 4\Delta$ SOLID-SOLID TRANSITION

We consider a simple model for the nucleation process. We assume that nucleation proceeds via the formation of a nucleus consisting of liquid-like and  $\Delta$ -solid-like particles. In addition, we assume that the nucleus is cylindrical with height  $H$  and consists of a cylindrical core of  $\Delta$ -solid-like particles surrounded by a cylindrical ring of liquid. We first consider two systems as shown in Fig. S5. System I contains the homogeneous metastable  $5\square$  phase, characterized by entropy  $S^I$ , volume  $V^I$ , and number of particles  $N$ , confined between two planar hard walls of total area  $A_{tot} = 2A$ , where  $A$  is the surface area of a single wall. System II contains a cluster consisting of  $N_L$  liquid particles and  $N_\Delta$  particles of the  $4\Delta$ -solid phase.

The difference between the Gibbs free energies of systems II and I is then given by

$$\begin{aligned} \Delta G = & (\mu_L - \mu_\square)N_L + (\mu_\Delta - \mu_\square)N_\Delta \\ & + (\gamma_{\Delta W} - \gamma_{\square W})A_\Delta + (\gamma_{LW} - \gamma_{\square W})A_L \\ & + \gamma_{\Delta L}A_{\Delta L} + \gamma_{L\square}A_{L\square}, \end{aligned} \quad (3)$$

where  $\gamma_{\alpha\beta}$  and  $A_{\alpha\beta}$  are the surface free energy (tension) and surface area for the  $\alpha - \beta$  interface respectively, where  $\alpha, \beta$  refer to  $L, \square, \Delta$  and the hard wall,  $W$ . For a cylindrical core of  $\Delta$ -solid-like particles surrounded by a cylindrical ring of liquid-like particles, we have  $A_\Delta = 2N_\Delta/(H\rho_\Delta)$ ,  $A_L = 2N_L/(H\rho_L)$ ,  $A_{\Delta L} = \sqrt{4\pi H/\rho_\Delta}\sqrt{N_\Delta}$  and  $A_{L\square} =$

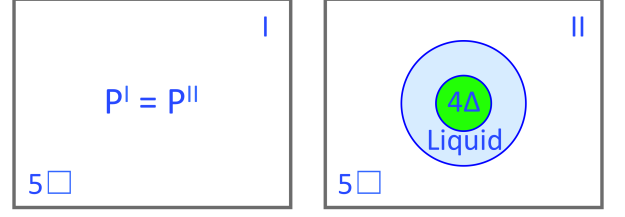


FIG. S5. A simple model for nucleation in a solid-solid transition. System I contains the homogeneous metastable  $5\square$ -solid phase confined between two planar hard walls. System II contains a cluster consisting of a  $4\Delta$ -solid-like core, surrounded by a liquid-like nucleus in a  $5\square$  solid confined between the same two walls.

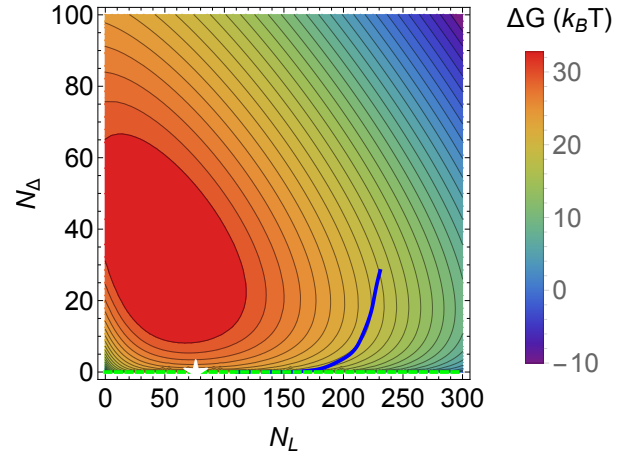


FIG. S6. Contour Plot of  $\beta\Delta G(N_L, N_\Delta)$  as obtained from classical nucleation theory for the  $5\square \rightarrow 4\Delta$  solid-solid transition at pressure  $P^* = 40$ . The green line represents a transition pathway along the  $N_\square$  axis at  $N_L = 0$ , and the blue line represents a transition pathway along a contour line of the surface.

$\sqrt{4\pi H/\rho_L}\sqrt{(\rho_L/\rho_\Delta)N_\Delta + N_L}$ . The Gibbs free-energy difference then reads

$$\begin{aligned} \Delta G = & \left[ \mu_L - \mu_\square + \frac{2}{H\rho_L}(\gamma_{LW} - \gamma_{\square W}) \right] N_L \\ & + \left[ \mu_\Delta - \mu_\square + \frac{2}{H\rho_\Delta}(\gamma_{\Delta W} - \gamma_{\square W}) \right] N_\Delta \\ & + \gamma_{\Delta L}\sqrt{\frac{4\pi H N_\Delta}{\rho_\Delta}} \\ & + \gamma_{L\square}\sqrt{\frac{4\pi H}{\rho_L} \left( \frac{\rho_L}{\rho_\Delta} N_\Delta + N_L \right)}. \end{aligned} \quad (4)$$

Figure S6 shows the free-energy landscape  $\Delta G(N_L, N_\Delta)$  obtained from Eq. 4 at pressure  $P^* = 40$ , where we have used the wall-fluid interfacial tension  $\beta\gamma_{LW}\sigma^2 = 1.990$ , the wall- $\Delta$  solid interfacial tension  $\beta\gamma_{\Delta W}\sigma^2 = 1.457$ , the wall- $\square$  solid interfacial tension  $\beta\gamma_{\square W}\sigma^2 = 2.106$  [1], and the liquid-solid interfacial

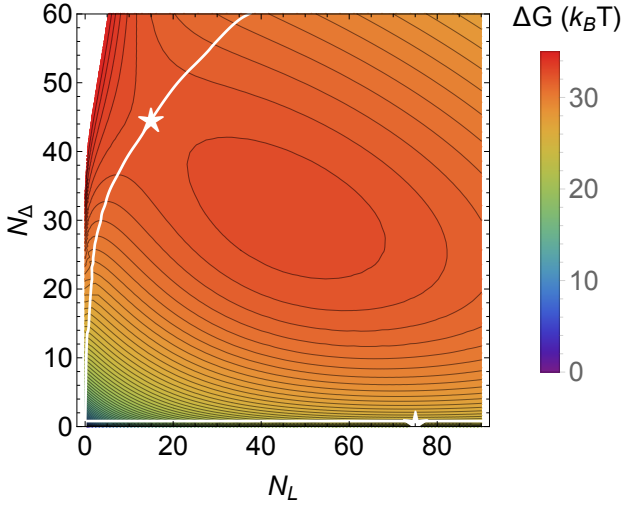


FIG. S7. Contour Plot of  $\beta\Delta G(N_L, N_\Delta)$  as obtained from the modified CNT model for the  $5\square \rightarrow 4\Delta$  solid-solid transition at pressure  $P^* = 40$  with parameters  $S = 0.03$ ,  $\xi = 0.5$  and  $\delta\epsilon = 0$ . The saddle points are marked by stars. White lines represent transition pathways along the valley floor and through the saddle points.

tension  $\beta\gamma_{LT}\sigma^2 = 0.62$  and  $\beta\gamma_{L\square}\sigma^2 = 0.62$  [3]. The free-energy surface shows that a high free-energy barrier stands between the  $5\square$ -solid and the  $4\Delta$ -solid phase (i.e. a path along the  $N_\square$  axis at  $N_L = 0$ ) due to the large free-energy cost associated with the formation of an interface between the two solid phases. This prevents a direct transformation of the  $5\square$ -solid to the  $4\Delta$ -solid phase. Instead, a lower free-energy path involves the formation of a liquid droplet, which beyond the saddle point grows spontaneously into the metastable liquid. The free-energy basin associated with the  $4\Delta$ -solid phase is separated from the liquid basin by a ridge on the free-energy surface. This free-energy surface is representative of a two-step nucleation mechanism where a liquid droplet first forms and grows before the solid phase nucleates, yielding two separate free-energy barriers. However, it is also interesting to note that clusters of the  $4\Delta$ -crystal can grow inside a critical liquid-like cluster without incurring an additional free-energy cost by following a path along the contour lines of the surface. The free energy surface obtained here differs from the one obtained in our free-energy calculations in Monte Carlo simulations using umbrella sampling.

#### IV. MODIFIED CNT MODEL

Now we consider two corrections of the classical nucleation theorem (CNT) model. The first correction term accounts for the disjoining pressure between the  $5\square$ -liquid and liquid- $4\Delta$  interfaces [4, 5]

$$\Delta G_{\square\text{-liquid-}\Delta} = A_{\square L} S \exp[-(r_L - r_\square)/\xi], \quad (5)$$

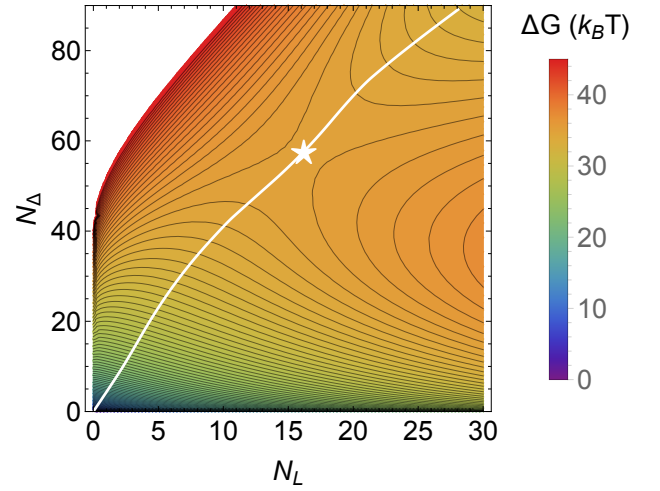


FIG. S8. Contour plot of  $\beta\Delta G(N_L, N_\Delta)$  as obtained from the modified CNT model for the  $5\square \rightarrow 4\Delta$  solid-solid transition at pressure  $P^* = 40$  with parameters  $S = 0.03$ ,  $\xi = 0.5$  and  $\delta\epsilon = 0.15$ . The saddle points are marked by stars. The white line represents transition pathways along the valley floor and through the saddle point.

where  $S = \gamma_{\square\Delta} - \gamma_{\Delta L} - \gamma_{L\square}$  is the spreading parameter,  $r$  is the nucleus radius, and  $\xi$  is the range of interaction between the two interfaces. For  $S = 0$ , the contribution of the disjoining pressure is zero. The second correction term is the strain energy  $E_{strain} \simeq N_L \Delta\epsilon$  associated with the expansion of the nucleus [6]. By adding the two correction terms to the CNT model, the free energy of formation of a nucleus is then given by

$$\begin{aligned} \Delta G = & \left[ \mu_L - \mu_\square + \Delta\epsilon + \frac{2}{H\rho_L}(\gamma_{LW} - \gamma_{\square W}) \right] N_L \\ & + \left[ \mu_\Delta - \mu_\square + \frac{2}{H\rho_\Delta}(\gamma_{\Delta W} - \gamma_{\square W}) \right] N_\Delta \\ & + \gamma_{\Delta L} \sqrt{\frac{4\pi H N_\Delta}{\rho_\Delta}} \\ & + \gamma_{L\square} \sqrt{\frac{4\pi H}{\rho_L} \left( \frac{\rho_L}{\rho_\Delta} N_\Delta + N_L \right)} \\ & + S \exp[-(r_L - r_\square)/\xi] \sqrt{\frac{4\pi H}{\rho_L} \left( \frac{\rho_L}{\rho_\Delta} N_\Delta + N_L \right)} \end{aligned} \quad (6)$$

As the values of  $\gamma_{\square\Delta}$ ,  $\xi$  and  $\Delta\epsilon$  are unknown, we treat them as free parameters in the modified CNT model. We set  $\xi = 0.5\sigma$  and find that the value of  $\xi$  does not affect the shape of the free-energy surface. Figure S7 is the free-energy surface of the modified CNT model with parameters  $\beta S\sigma^2 = 0.03$  and  $\Delta\epsilon = 0$ . There are two saddle points as denoted by the white asterisks in Figure S7, one for the pure liquid nucleus and the other for the liquid- $\Delta$  nucleus. As the value of the spreading parameter  $S$  increases, the saddle point of the liquid- $\Delta$

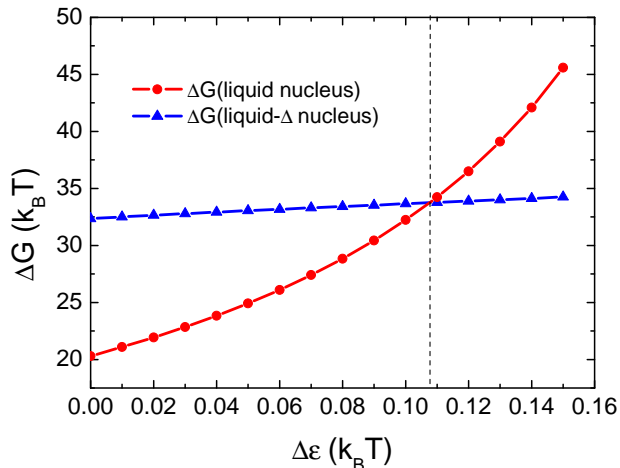


FIG. S9. The free energy barriers of the pure liquid nucleus and liquid- $\Delta$  nucleus as a function of strain energy  $\Delta\epsilon$  at  $P^* = 40$ . The other parameters are  $\beta S\sigma^2 = 0.03$  and  $\xi = 0.5\sigma$ .

nucleus moves towards the saddle point of the pure liquid nucleus, but the lowest free-energy pathway is always the one along the saddle point of the pure liquid involving the formation of a liquid nucleus.

Figure S8 is the free-energy surface of the modified CNT model with parameters  $S = 0.03$  and  $\beta\Delta\epsilon = 0.15$ , and thus includes a correction made to the strain energy of the  $5\Box$  crystal lattice. In this case, the free-energy barrier is  $\Delta G = 45.6k_B T$  for the pure liquid nucleus and  $\Delta G = 34.3k_B T$  for the liquid- $\Delta$  nucleus. Thus, the pathway along the liquid- $\Delta$  nucleus has the lowest free-energy barrier. Figure S9 shows the free-energy barriers of the pure liquid nucleus and of the liquid- $\Delta$  nucleus as a function of  $\Delta\epsilon$ . For  $\beta\Delta\epsilon < 0.108$ , the nucleation process is  $\Box \rightarrow \text{liquid} \rightarrow \Delta$ ; for  $\beta\Delta\epsilon > 0.108$ , the nucleation process is  $\Box \rightarrow (\text{liquid-}\Delta) \rightarrow \Delta$ . Note that the modified CNT model includes the possibility of liquid- $\Delta$  critical nucleus, the fluctuations leading to the growth of the critical cluster along the  $N_\Delta$  axis. But in our simulation,

a pure liquid nucleus is formed at the first stage of the nucleation, unlike in the simulations.

## V. NUCLEATION RATES FROM EDMD SIMULATIONS

For packing fraction  $\eta < 0.490$ , EDMD simulations can reveal every step of the nucleation process. The nucleation rate can be calculated by employing a combination of EDMD simulations and the mean first passage time analysis [7, 8]. At each packing fraction  $\eta = 0.480, 0.485, 0.488$  and  $0.490$ , we collect 3000 nucleation trajectories and calculate the mean first passage time,  $\tau(N_L)$ , for the formation of the cluster containing  $N_L$  liquid particles and the mean first passage time,  $\tau(N_\Delta)$ , for the formation of the cluster containing  $N_\Delta$   $\Delta$ -solid particles. These quantities are calculated independently, even though the triangular solid phase forms only in the presence of the liquid droplet. We estimate the size of the critical nucleus and the nucleation rate  $J$  by substituting the mean first passage times into the following expression [7, 8]:

$$\tau(N_i) = \frac{1}{2JV} \{1 + \text{erf}[C(N_i - N_{cri})]\}, \quad (7)$$

where  $i = L, \Delta$ ,  $N_{cri}$  is the critical size of the nucleus,  $J$  is the nucleation rate,  $V$  is the system volume,  $\text{erf}(x)$  is the error function, and  $C$  represents the curvature at the top of the nucleation barrier. Figure S10 shows the mean first passage times at  $\eta = 0.480, 0.485, \text{and } 0.488$ . The corresponding fitting parameters of Eq.(7) are presented in Table II. The critical size of the  $4\Delta$  nucleus does not change appreciably across  $\eta$ . In addition, we find that the nucleation rates  $J$  for the liquid-like and  $4\Delta$  solid-like clusters are very similar, which suggests that they describe the same nucleation barrier. The difference between the nucleation rates increases only slightly with decreasing  $\eta$ , which indicates that the  $\Delta$ -solid nucleates within a liquid nucleus.

[1] A. Fortini and M. Dijkstra, *J. Phys.: Condens. Matter* **18**, L371 (2006).  
 [2] K. Zahn and G. Maret, *Phys. Rev. Lett.* **85**, 3656 (2000).  
 [3] A. Härtel, M. Oettel, R. E. Rozas, S. U. Egelhaaf, J. Horbach, and H. Löwen, *Phys. Rev. Lett.* **108**, 226101 (2012).  
 [4] Y. S. Djikaev, R. Bowles, H. Reiss, K. Hämeri, A. Laaksonen, and M. Väkevä, *J. Phys. Chem. B* **105**, 7708 (2001).  
 [5] M. Iwamatsu, *J. Chem. Phys.* **134**, 164508 (2011).

[6] D. A. Porter, K. E. Easterling, and M. Y. Sherif, *Phase Transformations in Metals and Alloys* (CRC Press, Boca Raton, 2002).  
 [7] J. Wedekind, R. Strey, and D. Reguera, *J. Chem. Phys.* **126**, 134103 (2007).  
 [8] S. E. M. Lundrigan and I. Saika-Voivod, *J. Chem. Phys.* **131**, 104503 (2009).

$\eta$	liquid			$4\Delta$		
	$J_L(\tau/\sigma^3)$	$C_L$	$N_{cri,L}$	$J_\Delta(\tau/\sigma^3)$	$C_\Delta$	$N_{cri,\Delta}$
0.480	$3.53 \times 10^{-6}$	0.0437	395	$4.07 \times 10^{-6}$	0.246	5
0.485	$8.98 \times 10^{-7}$	0.0982	242	$9.90 \times 10^{-7}$	0.314	6
0.488	$2.40 \times 10^{-7}$	0.0157	199	$2.42 \times 10^{-7}$	0.319	6
0.490	$1.43 \times 10^{-7}$	0.0216	166	$1.43 \times 10^{-7}$	0.394	6

TABLE II. Fitting parameters of the mean first passage time for the liquid and the  $4\Delta$  solid at packing fractions  $\eta = 0.480$ ,  $0.485$ ,  $0.488$  and  $0.490$ .  $N_{cri}$  is the critical nucleus size.  $J_L$  and  $J_\Delta$  are the nucleation rate for the liquid and the  $4\Delta$  solid, respectively.  $C_L$  and  $C_\Delta$  denote the curvature at the top of the nucleation barrier.

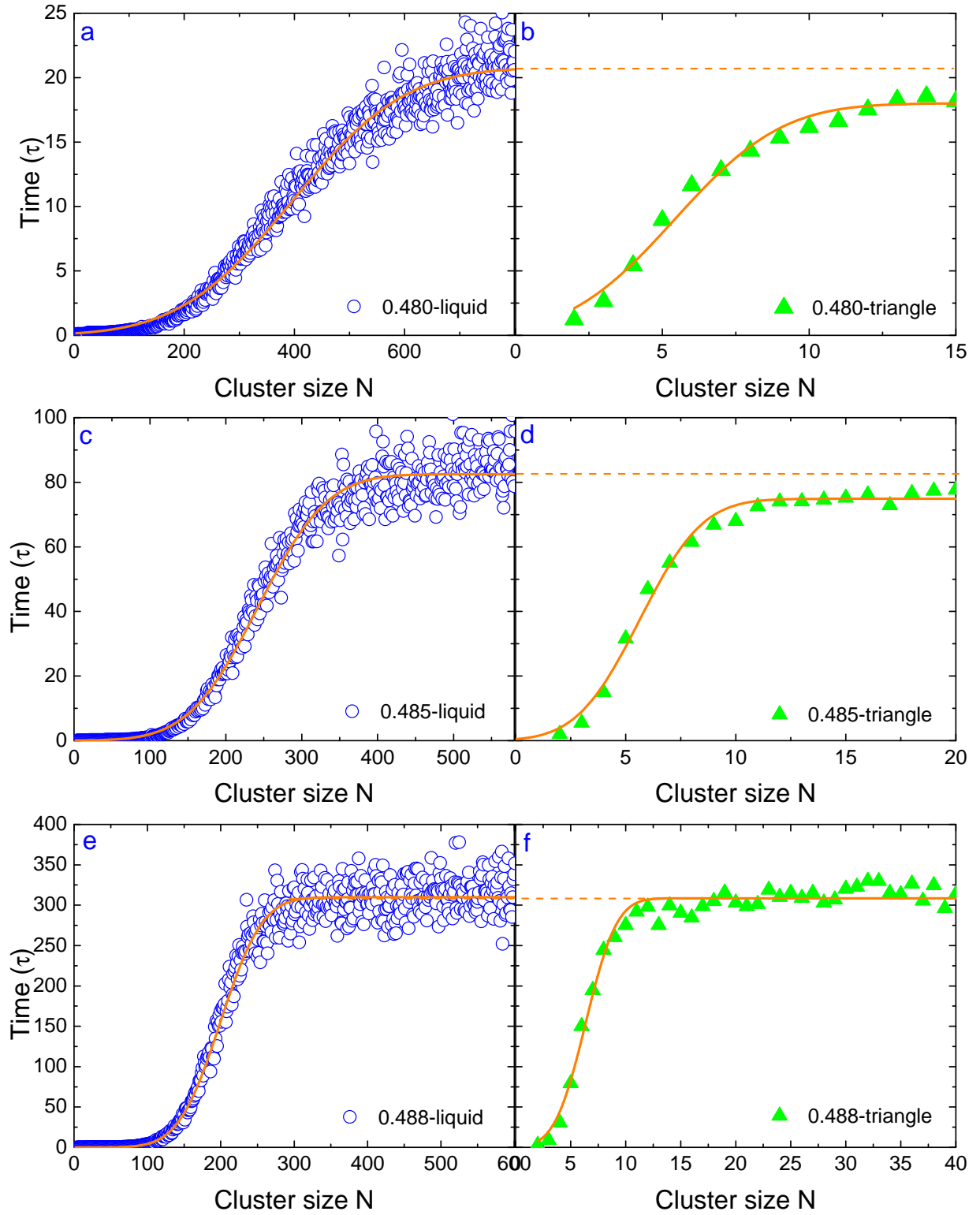


FIG. S10. The mean first passage time measured in EDMD time units for liquid-like (a, c, e) and  $4\Delta$ -solid-like (b, d, f) clusters as obtained from EDMD simulation at packing fractions  $\eta = 0.480$  (a, b),  $0.485$  (c, d) and  $0.488$  (e, f). Lines are fits of the mean first passage time using  $\frac{1}{2\sqrt{V}}\{1 + \text{erf}[C(N - N_{cri})]\}$ . The fitting parameters are shown in Table II.